68th International Astronautical Congress, Adelaide, Australia, 25-29 September 2017.

IAC-17,C1,2,4,x37573

Speed-Constrained Three-Axes Attitude Control Using Kinematic Steering

Hanspeter Schaub[a,*] and Scott Piggott[b]

[a] *Professor, Glenn L. Murphy Chair of Engineering, Department of Aerospace Engineering Sciences, University of Colorado, 431 UCB, Colorado Center for Astrodynamics Research, Boulder, CO 80309-0431.*, hanspeter.schaub@colorado.edu

[a] *Laboratory for Atmospheric and Space Physics, USA*, Scott.Piggott@lasp.colorado.edu

* Corresponding Author

Abstract

Spacecraft attitude control solutions typically are torque-level algorithms that simultaneously control both the attitude and angular velocity tracking errors. In contrast, robotic control solutions are kinematic steering commands where rates are treated as the control variable, and a servo-tracking control subsystem is present to achieve the desired control rates. In this paper kinematic attitude steering controls are developed where an outer control loop establishes a desired angular response history to a tracking error, and an inner control loop tracks the commanded body angular rates. The overall stability relies on the separation principle of the inner and outer control loops which must have sufficiently different response time scales. The benefit is that the outer steering law response can be readily shaped to a desired behavior, such as limiting the approach angular velocity when a large tracking error is corrected. A Modified Rodrigues Parameters implementation is presented that smoothly saturates the speed response. A robust nonlinear body rate servo loop is developed which includes integral feedback. This approach provides a convenient modular framework that makes it simple to interchange outer and inner control loops to readily setup new control implementations. Numerical simulations illustrate the expected performance for an aggressive reorientation maneuver subject to an unknown external torque.

1. Introduction

Three-axes spacecraft attitude control continues to be an active area of research. Extensive work has been performed on both nonlinear[1–6] and linear[7] attitude closed loop solutions. Such control solutions seek a stabilizing control torque which drives both the attitude and rate errors to zero. In essence, the linearized closed loop dynamics resemble mathematically a spring-mass-damper system. A particular challenge of the attitude feedback control development is handling complex rigid body kinematics simultaneously with the rigid body kinetics equations. For example, popular non-singular control solutions are developed for quaternions or Euler parameters[1,8] or Modified Rodrigues Parameters (MRPs).[3,9,10] If Lyapunov's direct method is employed to argue closed loop stability, care must be given in how the Lyapunov candidate function is formulated to provide insight into both the convergence of attitude and rate errors.

In contrast, the robotic control community often employs a very different approach. Their multi-link manipulator equations of motion are much more complex than those of a single rigid body. Instead of developing a torque level control to achieve the desired tracking, a kinematic steering control is implemented where the rates are treated as a control variable in an outer control loop.[11,12] To implement such a kinematic control, an inner speed control loop is required that has a much faster response time than the outer loop. Using the separation principle stability is examined by arguing that each loop individually is stable. In the field of spacecraft attitude control the use of steering laws is common when employing single-axis Control Moment Gyroscopes (CMGs). Here the control solution is written in terms of the gimble rates, not in terms of gimbal axis torques.[13–18] An inner control loop is assumed to track the desired gimble rate trajectory.

The presented attitude control technique is related to Backstepping Control method.[19] Here a desired kinematic response is created first which is then combined with a servo control. However, a benefit of the backstepping method is that the inner servo and outer kinematic stability is developed simultaneously, thus avoiding the need for the separation principle regarding the inner and outer loop response times. For example, Reference 20 presents an attitude control using the backstepping method for a regulation problem where all attitude and rate measures are driven towards zero. Here too the rates are smoothly saturated, but the stability proof is more complex due to the direct integration of the inner and outer loops. In contrast, if the separation principle is employed between the loops, then more general outer attitude control behaviors can be designed independent of the inner servo loop. For example, Reference 21 presents an interesting outer steering

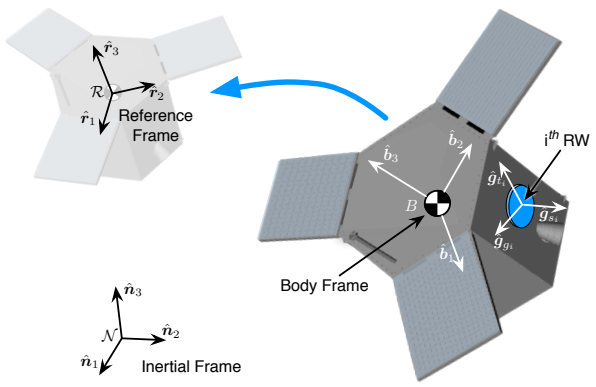

Fig. 1: Illustration of Coordinate Frame Definitions

loop that achieves autonomous conically constrained attitude motion. Here body fixed vectors are either force to remain outside a cone (i.e. sensor avoiding staring at sun) or inside a cone (i.e. solar panel normal remaining within a fixed angle relative to sun heading). This dual independent control loop setup is convenient in that it provides a readily modular design that allows the control loops to be interchanged in the software design process. The in-development Basilisk astrodynamics simulation software framework[1] creates a physics and control algorithm simulation framework where components can easily be exchanged. Reference 22 illustrates how Basilisk control guidance modules can be exchanged to create complex attitude guidance solutions.

This paper investigates creating kinematic steering laws to achieve novel three-axis attitude control laws suitable for general reference attitude tracking. Lyapunov's direct method is employed on the kinematic differential equation to establish necessary outer loop stability conditions. Specific implementations using the MRPs are developed that enforce pre-specified spacecraft rotational speed limits on the nominal closed loop control. Next, a spacecraft angular velocity vector based closed loop servo control is investigated for the inner speed servo loop. The nonlinear rate servo module employs robustness modifications using integral terms to reject unmodeled external torques. The modular control solution is implemented using the Basilisk framework to investigate how the overall control can be broken up into modular components.

2. Problem Statement

The kinematic control law is developed for a rigid spacecraft whose orientation is controlled through a cluster of N Reaction Wheels (RWs) as illustrated in Figure 1. The control goal is to drive a body-fixed frame $\mathcal{B} : \{\hat{\boldsymbol{b}}_1, \hat{\boldsymbol{b}}_2, \hat{\boldsymbol{b}}_3\}$ towards a time varying reference frame $\mathcal{R} : \{\hat{\boldsymbol{r}}_1, \hat{\boldsymbol{r}}_2, \hat{\boldsymbol{r}}_3\}$ as illustrated. The inertial frame is given by $\mathcal{N} : \{\hat{\boldsymbol{n}}_1, \hat{\boldsymbol{n}}_2, \hat{\boldsymbol{n}}_3\}$. The RW coordinate frame is given by $\mathcal{W}_i : \{\hat{\boldsymbol{g}}_{s_i}, \hat{\boldsymbol{g}}_{t_i}, \hat{\boldsymbol{g}}_{g_i}\}$. Here $\hat{\boldsymbol{g}}_{s_i}$ is a unique positive spin axis unit direction vector, while the other two axes complete a right-handed coordinate frame. Using MRPs at the attitude error measure, the overall control goal is $\boldsymbol{\sigma}_{\mathcal{B}/\mathcal{R}} \to 0$. The reference frame orientation $\boldsymbol{\sigma}_{\mathcal{R}/\mathcal{N}}$, angular velocity $\boldsymbol{\omega}_{\mathcal{R}/\mathcal{N}}$ and inertial angular acceleration $\dot{\boldsymbol{\omega}}_{\mathcal{R}/\mathcal{N}}$ are assumed to be known.

The rotational equations of motion of a rigid spacecraft with N RWs attached are given by[8]

$$[I_{\text{RW}}]\dot{\boldsymbol{\omega}} = -[\tilde{\boldsymbol{\omega}}]\left([I_{\text{RW}}]\boldsymbol{\omega} + [G_s]\boldsymbol{h}_s\right) - [G_s]\boldsymbol{u}_s + \boldsymbol{L} \quad (1)$$

where $\boldsymbol{u}_s$ is the set of RW motor torque, $\boldsymbol{L}$ is an external torque, and the inertia tensor $[I_{\text{RW}}]$ is defined as

$$[I_{\text{RW}}] = [I_s] + \sum_{i=1}^{N}\left(J_{t_i}\hat{\boldsymbol{g}}_{t_i}\hat{\boldsymbol{g}}_{t_i}^T + J_{g_i}\hat{\boldsymbol{g}}_{g_i}\hat{\boldsymbol{g}}_{g_i}^T\right) \quad (2)$$

The spacecraft inertial without the N RWs is $[I_s]$, while J_{s_i}, J_{t_i} and J_{g_i} are the RW inertias about the body fixed RW axis $\hat{\boldsymbol{g}}_{s_i}$ (RW spin axis), $\hat{\boldsymbol{g}}_{t_i}$ and $\hat{\boldsymbol{g}}_{g_i}$. The $3 \times N$ projection matrix $[G_s]$ is then defined as

$$[G_s] = \left[{}^{\mathcal{B}}\hat{\boldsymbol{g}}_{s_1} \cdots {}^{\mathcal{B}}\hat{\boldsymbol{g}}_{s_N}\right] \quad (3)$$

The RW inertial angular momentum vector $\boldsymbol{h}_s$ is defined as

$$h_{s_i} = J_{s_i}(\omega_{s_i} + \Omega_i) \quad (4)$$

Here Ω_i is the i^{th} RW spin relative to the spacecraft, and the body angular velocity is written in terms of body and RW frame components as

$$\boldsymbol{\omega} = \omega_1\hat{\boldsymbol{b}}_1 + \omega_2\hat{\boldsymbol{b}}_2 + \omega_3\hat{\boldsymbol{b}}_3 = \omega_{s_i}\hat{\boldsymbol{g}}_{s_i} + \omega_{t_i}\hat{\boldsymbol{g}}_{t_i} + \omega_{g_i}\hat{\boldsymbol{g}}_{g_i} \quad (5)$$

3. MRP Steering Law

3.1 Steering Law Stability Requirement

As is commonly done in robotic applications where the steering laws are of the form $\dot{\boldsymbol{x}} = \boldsymbol{u}$, this section derives a kinematic based attitude steering law. Let us consider the simple Lyapunov candidate function[8,10]

$$V(\boldsymbol{\sigma}_{\mathcal{B}/\mathcal{R}}) = 2\ln\left(1 + \boldsymbol{\sigma}_{\mathcal{B}/\mathcal{R}}^T\boldsymbol{\sigma}_{\mathcal{B}/\mathcal{R}}\right) \quad (6)$$

in terms of the MRP attitude tracking error $\boldsymbol{\sigma}_{\mathcal{B}/\mathcal{R}}$. Using the MRP differential kinematic equations[8]

$$\dot{\boldsymbol{\sigma}}_{\mathcal{B}/\mathcal{R}} = \frac{1}{4}[B(\boldsymbol{\sigma}_{\mathcal{B}/\mathcal{R}})]{}^{\mathcal{B}}\boldsymbol{\omega}_{\mathcal{B}/\mathcal{R}} = \frac{1}{4}\Big[(1-\sigma_{\mathcal{B}/\mathcal{R}}^2)[I_{3\times3}] + 2[\tilde{\boldsymbol{\sigma}}_{\mathcal{B}/\mathcal{R}}] + 2\boldsymbol{\sigma}_{\mathcal{B}/\mathcal{R}}\boldsymbol{\sigma}_{\mathcal{B}/\mathcal{R}}^T\Big]{}^{\mathcal{B}}\boldsymbol{\omega}_{\mathcal{B}/\mathcal{R}} \quad (7)$$

where $\sigma_{\mathcal{B}/\mathcal{R}}^2 = \boldsymbol{\sigma}_{\mathcal{B}/\mathcal{R}}^T\boldsymbol{\sigma}_{\mathcal{B}/\mathcal{R}}$, the time derivative of V is reduced to the elegantly simple form of

$$\dot{V} = \boldsymbol{\sigma}_{\mathcal{B}/\mathcal{R}}^T\left({}^{\mathcal{B}}\boldsymbol{\omega}_{\mathcal{B}/\mathcal{R}}\right) \quad (8)$$

[1] http://hanspeterschaub.info/bskMain.html

To create a kinematic steering law, let $\boldsymbol{\omega}_{\mathcal{B}^*/\mathcal{R}}$ be the desired angular velocity vector of this body orientation relative to the reference frame $\mathcal{R}$. The steering law requires a feedback control algorithm for the desired body rates $\boldsymbol{\omega}_{\mathcal{B}^*/\mathcal{R}}$ relative to the reference frame to make $\dot{V}$ in Eq. (8) negative definite. For this purpose, the general control formulation

$$^{\mathcal{B}}\boldsymbol{\omega}_{\mathcal{B}^*/\mathcal{R}} = -\boldsymbol{f}(\boldsymbol{\sigma}_{\mathcal{B}/\mathcal{R}}) \tag{9}$$

is proposed where $\boldsymbol{f}(\boldsymbol{\sigma})$ is an even function such that

$$\boldsymbol{\sigma}^T \boldsymbol{f}(\boldsymbol{\sigma}) > 0 \tag{10}$$

Substituting Eq. (9) into (8), the Lyapunov rate simplifies to a negative definite expression:

$$\dot{V} = -\boldsymbol{\sigma}_{\mathcal{B}/\mathcal{R}}^T \boldsymbol{f}(\boldsymbol{\sigma}_{\mathcal{B}/\mathcal{R}}) < 0 \tag{11}$$

The steering law in Eq. (9) allows for a broad range of kinematic response to tracking errors. The control designer can implement any even function $\boldsymbol{f}()$ while guaranteeing global asymptotic stability.

3.2 Saturated MRP Steering Law

This section explores particular implementations of $\boldsymbol{f}$ to consider different pointing scenarios. A very simple example is to set a linear steering law of the form

$$\boldsymbol{f}(\boldsymbol{\sigma}_{\mathcal{B}/\mathcal{R}}) = K_1 \boldsymbol{\sigma}_{\mathcal{B}/\mathcal{R}} \tag{12}$$

where $K_1 > 0$. This yields a kinematic control where the desired body rates are proportional to the MRP attitude error measure. As the MRP error measure norm is bounded by unity, the kinematic speed command is also bounded. However, it is monotonically increasing until the maximum error of 180° is reached.

If the commanded rate should saturate at an earlier tracking error angle, then $\boldsymbol{f}()$ could be defined as

$$\boldsymbol{f}(\boldsymbol{\sigma}_{\mathcal{B}/\mathcal{R}}) = \begin{cases} K_1\sigma_i & \text{if } |K_1\sigma_i| \leqslant \omega_{\text{max}} \\ \omega_{\text{max}}\text{sgn}(\sigma_i) & \text{if } |K_1\sigma_i| > \omega_{\text{max}} \end{cases} \tag{13}$$

where $\boldsymbol{\sigma}_{\mathcal{B}/\mathcal{R}} = (\sigma_1, \sigma_2, \sigma_3)^T$. A smoothly saturating function is given by

$$f(\sigma_i) = \arctan\left(\sigma_i \frac{K_1\pi}{2\omega_{\text{max}}}\right)\frac{2\omega_{\text{max}}}{\pi} \tag{14}$$

where

$$\boldsymbol{f}(\boldsymbol{\sigma}_{\mathcal{B}/\mathcal{R}}) = \begin{pmatrix} f(\sigma_1) \\ f(\sigma_2) \\ f(\sigma_3) \end{pmatrix} \tag{15}$$

As $\sigma_i \to \infty$ the function f smoothly converges to a maximum rate command of $\pm\omega_{\text{max}}$. For small $|\boldsymbol{\sigma}_{\mathcal{B}/\mathcal{R}}|$, this function linearizes to

$$\boldsymbol{f}(\boldsymbol{\sigma}_{\mathcal{B}/\mathcal{R}}) \approx K_1\boldsymbol{\sigma}_{\mathcal{B}/\mathcal{R}} + \text{ H.O.T} \tag{16}$$

If the MRP shadow set parameters are used to avoid the MRP singularity at 360°, then $|\boldsymbol{\sigma}_{\mathcal{B}/\mathcal{R}}|$ is upper limited by 1. To control how rapidly the rate commands approach the ω_{max} limit, Eq. (14) is modified to include a cubic term:

$$f(\sigma_i) = \arctan\left((K_1\sigma_i + K_3\sigma_i^3)\frac{\pi}{2\omega_{\text{max}}}\right)\frac{2\omega_{\text{max}}}{\pi} \tag{17}$$

The order of the polynomial must be odd to keep $\boldsymbol{f}()$ an even function. A nice feature of Eq. (17) is that the control rate is saturated individually about each axis. If the smoothing component is removed to reduce this to a bang-band rate control, then this would yield a Lyapunov optimal control which minimizes $\dot{V}$ subject to the allowable rate constraint ω_{max}.

Figure 2 illustrates how the parameters ω_{max}, K_1 and K_3 impact the steering law behavior. The maximum steering law rate commands are easily set through the ω_{max} parameters. The gain K_1 controls the linear stiffness when the attitude errors have become small, while K_3 controls how rapidly the steering law approaches the speed command limit.

The required velocity servo loop design is aided by knowing the body-frame derivative of $^{\mathcal{B}}\boldsymbol{\omega}_{\mathcal{B}^*/\mathcal{R}}$ to implement a feed-forward component. Using the $\boldsymbol{f}()$ function definition in Eq. (15), this requires the time derivatives of $f(\sigma_i)$.

$$\begin{aligned} \frac{^{\mathcal{B}}\text{d}(^{\mathcal{B}}\boldsymbol{\omega}_{\mathcal{B}^*/\mathcal{R}})}{\text{d}t} &= \boldsymbol{\omega}'_{\mathcal{B}^*/\mathcal{R}} \\ &= -\frac{\partial \boldsymbol{f}}{\partial \boldsymbol{\sigma}_{\mathcal{B}^*/\mathcal{R}}}\dot{\boldsymbol{\sigma}}_{\mathcal{B}^*/\mathcal{R}} = -\begin{pmatrix} \frac{\partial f}{\partial \sigma_1}\dot{\sigma}_1 \\ \frac{\partial f}{\partial \sigma_2}\dot{\sigma}_2 \\ \frac{\partial f}{\partial \sigma_3}\dot{\sigma}_3 \end{pmatrix} \end{aligned} \tag{18}$$

where

$$\begin{aligned} \dot{\boldsymbol{\sigma}}_{\mathcal{B}^*/\mathcal{R}} &= \begin{pmatrix} \dot{\sigma}_1 \\ \dot{\sigma}_2 \\ \dot{\sigma}_3 \end{pmatrix} = \frac{1}{4}[B(\boldsymbol{\sigma}_{\mathcal{B}^*/\mathcal{R}})]^{\mathcal{B}}\boldsymbol{\omega}_{\mathcal{B}^*/\mathcal{R}} \\ &= -\frac{1}{4}[B(\boldsymbol{\sigma}_{\mathcal{B}^*/\mathcal{R}})]\boldsymbol{f}(\boldsymbol{\sigma}_{\mathcal{B}^*/\mathcal{R}}) \end{aligned} \tag{19}$$

Using the general $f()$ definition in Eq. (17), its sensitivity with respect to σ_i is

$$\frac{\partial f}{\partial \sigma_i} = \frac{(K_1 + 3K_3\sigma_i^2)}{1 + (K_1\sigma_i + K_3\sigma_i^3)^2\left(\frac{\pi}{2\omega_{\text{max}}}\right)^2} \tag{20}$$

Next, let us investigate the closed loop performance. For small errors, assuming a perfect rate-servo subsystem, the closed loop dynamics is given in Eq. (16). Using the MRP differential kinematic equation approximation $\dot{\boldsymbol{\sigma}} = \boldsymbol{\omega}/4$, this is rewritten as the first order differential equation

$$\dot{\boldsymbol{\sigma}}_{\mathcal{B}^*/\mathcal{R}} = -\frac{K_1}{4}\boldsymbol{\sigma}_{\mathcal{B}^*/\mathcal{R}} \tag{21}$$

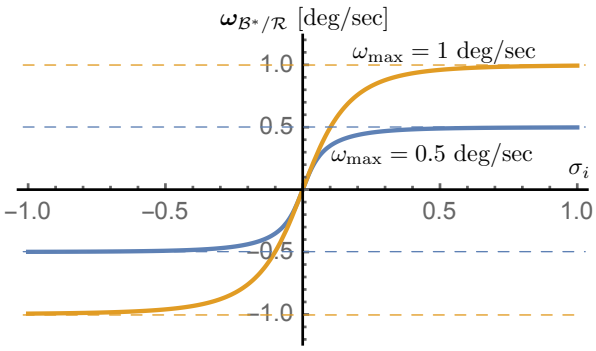

(a) $\omega_{\max}$ dependency with $K_1 = 0.1$, $K_3 = 1$

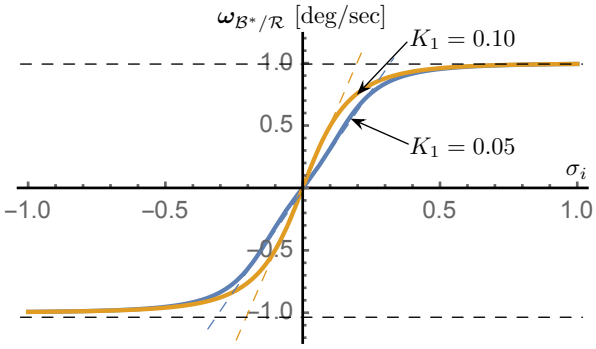

(b) K_1 dependency with $\omega_{\max} = 1^\circ/s$, $K_3 = 1$

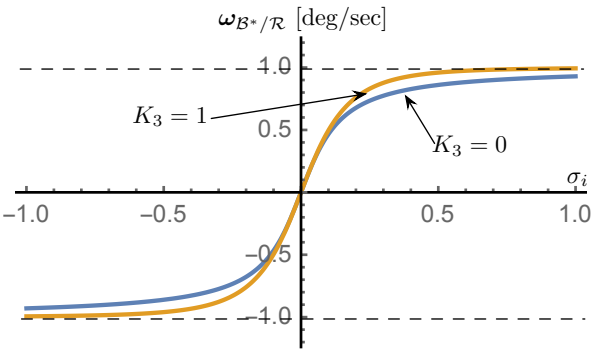

(c) K_3 dependency with $\omega_{\max} = 1^\circ/s$, $K_1 = 0.1$

Fig. 2: Illustrations of MRP Steering Parameters Influence.

The corresponding half-life of the exponential outer closed-loop dynamics is

$$T_{1/2,\text{Outer}} = \frac{4\ln 2}{K_1} \tag{22}$$

When picking the K_1 gain, it is critical that this decay time is sufficiently larger than the decay time of the rate-servo inner loop.

4. Angular Velocity Servo Sub-System

4.1 Servo with Angular Rate Error Integral Measure

To implement the kinematic steering control, a servo sub-system must be included which produces the required torques to make the actual body rates track the desired body rates. The angular velocity tracking error vector is defined as

$$\delta\boldsymbol{\omega} = \boldsymbol{\omega}_{\mathcal{B}/\mathcal{B}^*} = \boldsymbol{\omega}_{\mathcal{B}/\mathcal{N}} - \boldsymbol{\omega}_{\mathcal{B}^*/\mathcal{N}} \tag{23}$$

where the $\mathcal{B}^*$ frame is the desired body frame from the kinematic steering law. Note that

$$\boldsymbol{\omega}_{\mathcal{B}^*/\mathcal{N}} = \boldsymbol{\omega}_{\mathcal{B}^*/\mathcal{R}} + \boldsymbol{\omega}_{\mathcal{R}/\mathcal{N}} \tag{24}$$

where $\boldsymbol{\omega}_{\mathcal{R}/\mathcal{N}}$ is obtained from the attitude navigation solution, and $\boldsymbol{\omega}_{\mathcal{B}^*/\mathcal{R}}$ is the kinematic steering rate command. To create a rate-servo system that is robust to unmodeld torque biases, the state $\boldsymbol{z}$ is defined as:

$$\boldsymbol{z} = \int_{t_0}^{t_f} {}^{\mathcal{B}}\delta\boldsymbol{\omega}\, \mathrm{d}t \tag{25}$$

The rate servo Lyapunov function is defined as

$$V_{\boldsymbol{\omega}}(\delta\boldsymbol{\omega}, \boldsymbol{z}) = \frac{1}{2}\delta\boldsymbol{\omega}^T[I_{\text{RW}}]\delta\boldsymbol{\omega} + \frac{1}{2}\boldsymbol{z}^T[K_I]\boldsymbol{z} \tag{26}$$

where the vector $\delta\boldsymbol{\omega}$ and tensor $[I_{\text{RW}}]$ are assumed to be given in body frame components, $[K_i]$ is a symmetric positive definite matrix. The time derivative of this Lyapunov function is

$$\dot{V}_{\boldsymbol{\omega}} = \delta\boldsymbol{\omega}^T\left([I_{\text{RW}}]\delta\boldsymbol{\omega}' + [K_I]\boldsymbol{z}\right) \tag{27}$$

Using the identities $\boldsymbol{\omega}'_{\mathcal{B}/\mathcal{N}} = \dot{\boldsymbol{\omega}}_{\mathcal{B}/\mathcal{N}}$ and $\boldsymbol{\omega}'_{\mathcal{R}/\mathcal{N}} = \dot{\boldsymbol{\omega}}_{\mathcal{R}/\mathcal{N}} - \boldsymbol{\omega}_{\mathcal{B}/\mathcal{N}} \times \boldsymbol{\omega}_{\mathcal{R}/\mathcal{N}}$,[8] the body frame derivative of $\delta\boldsymbol{\omega}$ is

$$\delta\boldsymbol{\omega}' = \dot{\boldsymbol{\omega}}_{\mathcal{B}/\mathcal{N}} - \boldsymbol{\omega}'_{\mathcal{B}^*/\mathcal{R}} - \dot{\boldsymbol{\omega}}_{\mathcal{R}/\mathcal{N}} + \boldsymbol{\omega}_{\mathcal{B}/\mathcal{N}} \times \boldsymbol{\omega}_{\mathcal{R}/\mathcal{N}} \tag{28}$$

Substituting Eqs. (1) and (28) into the $\dot{V}_{\boldsymbol{\omega}}$ expression in Eq. (27) yields

$$\begin{aligned}\dot{V}_{\boldsymbol{\omega}} = \delta\boldsymbol{\omega}^T\Big(&- [\tilde{\boldsymbol{\omega}}_{\mathcal{B}/\mathcal{N}}]\left([I_{\text{RW}}]\boldsymbol{\omega}_{\mathcal{B}/\mathcal{N}} + [G_s]\boldsymbol{h}_s\right) \\ &- [G_s]\boldsymbol{u}_s + \boldsymbol{L} + [K_I]\boldsymbol{z} \\ &- [I_{\text{RW}}](\boldsymbol{\omega}'_{\mathcal{B}^*/\mathcal{R}} + \dot{\boldsymbol{\omega}}_{\mathcal{R}/\mathcal{N}} - \boldsymbol{\omega}_{\mathcal{B}/\mathcal{N}} \times \boldsymbol{\omega}_{\mathcal{R}/\mathcal{N}})\Big)\end{aligned} \tag{29}$$

Let $[P]^T = [P] >$ be a symmetric positive definite rate feedback gain matrix. The servo rate feedback control is defined as

$$\begin{aligned}[G_s]\boldsymbol{u}_s = &[P]\delta\boldsymbol{\omega} + [K_I]\boldsymbol{z} \\ &- [\tilde{\boldsymbol{\omega}}_{\mathcal{B}^*/\mathcal{N}}]\left([I_{\text{RW}}]\boldsymbol{\omega}_{\mathcal{B}/\mathcal{N}} + [G_s]\boldsymbol{h}_s\right) \\ &- [I_{\text{RW}}](\boldsymbol{\omega}'_{\mathcal{B}^*/\mathcal{R}} + \dot{\boldsymbol{\omega}}_{\mathcal{R}/\mathcal{N}} - \boldsymbol{\omega}_{\mathcal{B}/\mathcal{N}} \times \boldsymbol{\omega}_{\mathcal{R}/\mathcal{N}}) + \boldsymbol{L}\end{aligned} \tag{30}$$

Defining the right-hand-side as $\boldsymbol{L}_r$, this is rewritten in compact form as

$$[G_s]\boldsymbol{u}_s = \boldsymbol{L}_r \tag{31}$$

The array of RW motor torques can be solved with the typical minimum norm inverse

$$\boldsymbol{u}_s = [G_s]^T \left([G_s][G_s]^T\right)^{-1} \boldsymbol{L}_r \tag{32}$$

To analyze the stability of this rate servo control, the $[G_s]\boldsymbol{u}_s$ expression in Eq. (30) is substituted into the Lyapunov rate expression in Eq. (29).

$$\begin{aligned}\dot{V}_\omega &= \delta\boldsymbol{\omega}^T\Big(- [P]\delta\boldsymbol{\omega} - [\tilde{\boldsymbol{\omega}}_{\mathcal{B}/\mathcal{N}}]\left([I_{\text{RW}}]\boldsymbol{\omega}_{\mathcal{B}/\mathcal{N}} + [G_s]\boldsymbol{h}_s\right) \\ &\quad + [\tilde{\boldsymbol{\omega}}_{\mathcal{B}^*/\mathcal{N}}]\left([I_{\text{RW}}]\boldsymbol{\omega}_{\mathcal{B}/\mathcal{N}} + [G_s]\boldsymbol{h}_s\right)\Big) \\ &= \delta\boldsymbol{\omega}^T\Big(- [P]\delta\boldsymbol{\omega} - [\widetilde{\delta\boldsymbol{\omega}}]\left([I_{\text{RW}}]\boldsymbol{\omega}_{\mathcal{B}/\mathcal{N}} + [G_s]\boldsymbol{h}_s\right)\Big) \\ &= -\delta\boldsymbol{\omega}^T[P]\delta\boldsymbol{\omega} < 0 \end{aligned} \tag{33}$$

Thus, in the absence of unmodeled torques, the servo control in Eq. (30) is asymptotically stabilizing in rate tracking error $\delta\boldsymbol{\omega}$.

Next, the servo robustness to unmodeled external torques is investigated. Let us assume that the external torque vector $\boldsymbol{L}$ in Eq. (1) only approximates the true external torque, and the unmodeled component is given by $\Delta\boldsymbol{L}$. Substituting the true equations of motion and the same servo control in Eq. (30) into the Lyapunov rate expression in Eq. (27) leads to

$$\dot{V}_\omega = -\delta\boldsymbol{\omega}^T[P]\delta\boldsymbol{\omega} + \delta\boldsymbol{\omega}^T\Delta\boldsymbol{L} \tag{34}$$

This $\dot{V}_\omega$ is no longer negative definite due to the underdetermined sign of the $\delta\boldsymbol{\omega}^T\Delta\boldsymbol{L}$ components. Equating the Lyapunov rates in Eqs. (27) and (34) yields the following servo closed loop dynamics:

$$[I_{\text{RW}}]\delta\boldsymbol{\omega}' + [P]\delta\boldsymbol{\omega} + [K_I]\boldsymbol{z} = \Delta\boldsymbol{L} \tag{35}$$

Assuming that $\Delta\boldsymbol{L}$ is either constant as seen by the body frame, or at least varies slowly, then taking a body-frame time derivative of Eq. (35) is

$$[I_{\text{RW}}]\delta\boldsymbol{\omega}'' + [P]\delta\boldsymbol{\omega}' + [K_I]\delta\boldsymbol{\omega} = \Delta\boldsymbol{L}' \approx 0 \tag{36}$$

As $[I_{\text{RW}}]$, $[P]$ and $[K_I]$ are all symmetric positive definite matrices, these linear differential equations are stable, and $\delta\boldsymbol{\omega} \to 0$ given that assumption that $\Delta\boldsymbol{L}' \approx 0$.

Next the performance of this inner rate servo-loop is considered. Equating Eq. (27) and (33), the rate-servo closed loop equations are given as the linear expression

$$[I_{\text{RW}}]\delta\boldsymbol{\omega}' + [P]\delta\boldsymbol{\omega} + [K_I]\boldsymbol{z} = \boldsymbol{0} \tag{37}$$

To simplify the following analysis, assume that $[I_{\text{RW}}] = \text{diag}(I_1, I_2, I_3)$, $[P] = \text{diag}(P_1, P_2, P_3)$ and $[K_I] = \text{diag}(K_{I,1}, K_{I,2}, K_{I,3})]$ are diagonal matrices matrices. The roots of the characteristic equation of Eq. (37) are

$$s_{1/2} = \frac{-P_i \pm \sqrt{P_i^2 - 4I_iK_{I,i}}}{2I_i} \tag{38}$$

If $K_{I,i} = 0$ and the integral feedback is turned off, then the root simplifies to

$$s = -\frac{P_i}{I_i} \tag{39}$$

where the inner rate servo loop half life is given by

$$T_{1/2,\text{Inner}} = \frac{I_i \ln 2}{P_i} \tag{40}$$

Note that without the integral feedback the closed loop response is always an exponentially decaying behavior. The rate feedback gains P_i must be chosen that that $T_{1/2,\text{Inner}} \ll T_{1/2,\text{Outer}}$ and the separation principle guaranteeing the stability of both the out and inner control loops is valid.

If integral feedback is enabled, then two exponentially decaying roots appear if $K_{I,i} < P_i^2/(2I_i)$. For larger $K_{I,i}$ values the servo response becomes under-damped and oscillatory.

4.2 Linearized Closed Loop Dynamics Analysis

The closed-loop control in Eq. (30) is shown to be asymptotically stabilizing in the presence of a body-fixed disturbance torque. However, this stability assumes the separation principle holds and that the outer control decay time constant is much larger than the inner rate-servo loop decay time constant. In the absence of an unmodeled control torque, the rate-servo closed loop dynamics are given by

$$[I_{\text{RW}}]\delta\boldsymbol{\omega}' + [P]\delta\boldsymbol{\omega} + [K_I]\boldsymbol{z} = 0 \tag{41}$$

To develop the linearized Closed Loop Dynamics (CLD) the reference motion $\mathcal{R}$ is set to be identical to the inertial frame $\mathcal{N}$. Here $\boldsymbol{\omega}_{\mathcal{R}/N} = \dot{\boldsymbol{\omega}}_{\mathcal{R}/N} = 0$. Note that

$$\delta\boldsymbol{\omega} = \boldsymbol{\omega}_{\mathcal{B}/N} - \boldsymbol{\omega}_{\mathcal{B}^*/N} = \boldsymbol{\omega}_{\mathcal{B}/N} + \boldsymbol{f}(\boldsymbol{\sigma}_{\mathcal{B}/N}) \tag{42}$$

Next, assume that the inertia tensor is $[I_{\text{RW}}] = \text{diag}(I_1, I_2, I_3)$, and the gain matrices are $[P] = \text{diag}(P_1, P_2, P_3)$ and $[K_I] = \text{diag}(K_{I,1}, K_{I,2}, K_{I,3})$. Using ${}^{\mathcal{B}}\boldsymbol{\omega}_{\mathcal{B}/N} = (\omega_1, \omega_2, \omega_3)$ and $\boldsymbol{\sigma}_{\mathcal{B}/N} = (\sigma_1, \sigma_2, \sigma_3)$ the CLD is then written as

$$I_i\dot{\omega}_i + I_i\dot{f}(\sigma_i) + P_i(\omega_i + f(\sigma_i)) + K_{I,i}\int(\omega_i + f(\sigma_i))\text{d}t = 0 \tag{43}$$

Using small angular departure assumptions, the following linearizations hold:

$$f(\sigma_i) \approx K_1\sigma_i \tag{44a}$$

$$\omega_i \approx 4\dot{\sigma}_i \tag{44b}$$

The time derivative of the $f()$ function uses Eq. (19) to find

$$\begin{aligned}\dot{f}(\sigma_i) \approx K_1\dot{\sigma}_i &= K_1\frac{\omega_{\mathcal{B}^*/N,i}}{4} \\ &= \frac{K_1}{4}(-K_1\sigma_i) = -\frac{K_1^2}{4}\sigma_i \end{aligned} \tag{45}$$

The revised linearized CLD are now

$$4I_i\ddot{\sigma}_i + 4P_i\dot{\sigma}_i + \left(PK_1 + 4K_I - \frac{I_iK_1^2}{4}\right)\sigma_i + K_{I,i}K_1\int \sigma_i \mathrm{d}t = 0 \quad (46)$$

The roots of the associate characteristic equation are

$$s_1 \to -\frac{K_1}{4} \quad (47a)$$

$$s_{2,3} \to \frac{1}{2}\left(\kappa \pm \sqrt{\kappa^2 - 4\frac{K_{I,i}}{I_i}}\right) \quad (47b)$$

where

$$\kappa = -\frac{P_i}{I_i} + \frac{K_1}{4} \quad (48)$$

For the CLD to be stable, note that P_i and K_1 must be chosen such that

$$\frac{P_i}{I_i} > \frac{K_1}{4} \quad (49)$$

Using the results in Eq. (22) and (40), this stability condition is equivalent to saying

$$T_{1/2,\text{Inner}} < T_{1/2,\text{Outer}} \quad (50)$$

Next, consider the case where a large gain K_1 is chosen to increase the CLD stiffness, but it violates the above stability condition. For example, such a setup would be attractive for trajectory correction maneuvers where even a small thruster miss-alignment will cause a large torque onto the spacecraft. Tight pointing tolerances during a burn require the control to rapidly respond to a pointing error, and thus necessitate a large K_1 value. In this case the control could be modified by removing the outer-loop feed-forward component to be

$$\begin{aligned}[G_s]\boldsymbol{u}_s = {} & [P]\delta\boldsymbol{\omega} + [K_I]\boldsymbol{z} \\ & - [\tilde{\boldsymbol{\omega}}_{\mathcal{B}^*/\mathcal{N}}]\left([I_{\text{RW}}]\boldsymbol{\omega}_{\mathcal{B}/\mathcal{N}} + [G_s]\boldsymbol{h}_s\right) \\ & - [I_{\text{RW}}](\dot{\boldsymbol{\omega}}_{\mathcal{R}/\mathcal{N}} - \boldsymbol{\omega}_{\mathcal{B}/\mathcal{N}} \times \boldsymbol{\omega}_{\mathcal{R}/\mathcal{N}}) + \boldsymbol{L}\end{aligned} \quad (51)$$

Not having this feed forward term included means the $\delta\boldsymbol{\omega}$ tracking won't be perfect as long as $\dot{f}$ is not zero. In essence, the neglected outer-loop feed-forward component is treated as an unmodeled torque influence on the CLD. However, in this case the linearized CLD become

$$4I_i\ddot{\sigma}_i + 4P_i\dot{\sigma}_i + (PK_1 + 4K_I)\sigma_i + K_{I,i}K_1\int \sigma_i \mathrm{d}t = 0 \quad (52)$$

which are guaranteed locally stable for any positive K_1 and P gain values as long as the integral gain is sufficiently small. Note that if $K_1 > 4P_i/I_i$ then the control will no longer act as the earlier outlined steering law as the inner loop is too slow to track the kinematic steering command. However, the resulting CLD is a stable response if the outer-loop feedforward component is neglected. This allows for the CLD stiffness to be increased, resulting in a very stiff control response about a reference motion.

Table 1: Numerical Attitude Simulation Parameters

Symbols	Value(s)	Units
(I_1, I_2, I_3)	[500.0, 300.0, 200.0]	kgm^2
${}^{\mathcal{B}}\hat{\boldsymbol{g}}_{s_1}$	[1, 0, 0]	
${}^{\mathcal{B}}\hat{\boldsymbol{g}}_{s_2}$	[0, 1, 0]	
${}^{\mathcal{B}}\hat{\boldsymbol{g}}_{s_3}$	[0, 0, 1]	
J_{s_i}	0.0796	kgm^2
u_{max}	0.2	Nm
$\boldsymbol{\Omega}$	[100.0, 200.0, 300.0]	RPM
$\boldsymbol{L}$	[0.01, -0.01, 0.005]	Nm
K_1	0.05	
K_3	0.75	
ω_{max}	1.0	deg/s
P	150.0	Nms
K_i	5.0	Nm

5. Numerical Simulations

5.1 General Simulation Setup Using Basilisk

The performance of the outer- and inner-loop attitude control strategies are demonstrated next using the MRP formulation using a rigid spacecraft with three reaction wheels attached. The nominal spacecraft and control parameters are shown in Table 1. A classical reaction wheel alignment is assumed with the spin axes $\hat{\boldsymbol{g}}_{s_i}$ aligned with the principal body frame. The reaction wheel speeds are given non-zero initial momentum values, and a body-fixed unmodeled external torque is included. This torque is not fed forward in any of the feedback control scenarios discussed next. The control objective is a tracking problem to align the body frame with the Hill orbit frame. The Earth orbit is defined through a semin-major axis of 10,000km, an eccentricity of 0.1, an inclination angle of 0.1°, ascending node of 48.2°, argument of periapses of 347.8°and an initial true anomaly of 85.3°. The dynamical differential equations are integrated using a fourth order Runge-Kutta scheme using a 0.1s integration and control update step.

The Basilisk (BSK) astrodynamics simulation framework[23] is used to simulate the spacecraft dynamics and implement the MRP steering control solution in a modular fashion. A flow-diagram of the BSK modules used are shown in Figure 3. The rigid spacecraft hub component is connected to three balanced Reaction Wheel (RW) effectors, as well as a disturbance torque module for the unmodeled body-fixed torque. The simulation is setup to illustrate a regular problem where $\mathcal{B} \to \mathcal{R}$ through the `hillPoint()` module. The attitude tracking error model takes the actual and reference attitude states

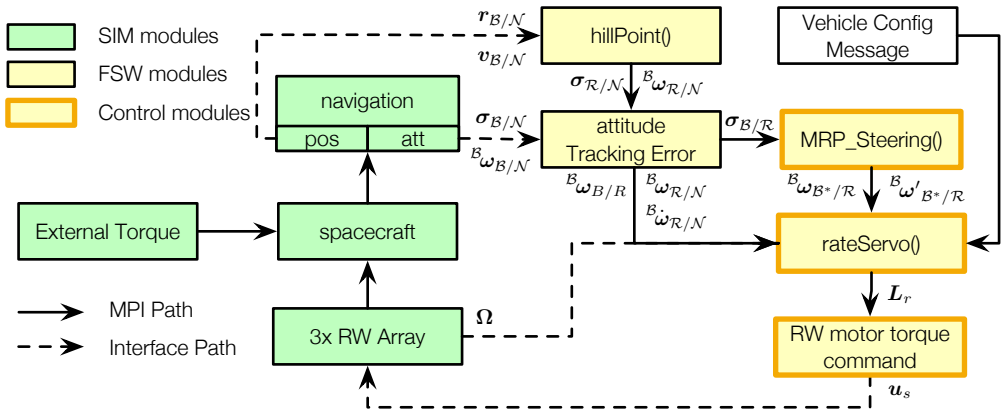

Fig. 3: Basilisk Simulation Setup Illustration

and outputs the tracking error information. The presented MRP steering control is implemented through three discrete modules shown with a thick orange border. The outer steering loop rate control in Eq. (9) is the output of the MRP Steering module. The rateServo() modules computer the body-relative control torque vector solution $\boldsymbol{L}_r$ in Eq. (30). The final module maps $\boldsymbol{L}_r$ to the set of RW motor torques $\boldsymbol{u}_s$. As the 3 RW axes line up with the $\mathcal{B}$ frame, this is a simple identity mapping for this scenario. The BSK torque mapping module implements a standard minimum norm inverse if more than 3 RW are controlled. The simulated communication paths (dashed lines) provide the rateServo() module with the RW speeds, and pass on the RW motor torques $\boldsymbol{u}_s$ to the RW torque inputs.

No measurement noise is intentionally being modeled here to illustrate the expected asymptotic performance of the steering control implementation, and robustness to unmodeled body-fixed external disturbance forces. As this control reduces to a classical linear control solution for small departures, standard noise impact theories from linear control apply here as well for small departure motions.

5.2 Large Maneuver and Detumble Response

The first simulation considers a very large reorientation maneuver where the initial body and inertial frame differ by a principal angle of 159.7°, expressed as $\boldsymbol{\sigma}_{\mathcal{B}/\mathcal{N}}(t_0) = (0.5, 0.6, -0.3)$. The large angular motion will illustrate the desired angular rates reaching $\omega_{\max}$ when far away from the desired attitude, and then exponentially converging to the final orientation. In addition, an initial tumble rate of $\boldsymbol{\omega}_{\mathcal{B}/\mathcal{N}}(t_0) = (0.01, -0.01, -0.01)$ rad/s is provided to illustrate the rate servo performance which must compensate for large initial tumble rates. Note that no reference rate smoothing is employed here as might be added in an actual application. This is to illustrate how robustly the rates are driven to the desired values even if the actuator mechanism saturates for a short period.

The nominal control gains shown in Table 1 yield an outer time decay constant of about 55.45 seconds, while the inner rate servo loop (without integral feedback) has a much faster time decay constant of about 1.84 seconds. This wide margin in the outer and inner loop response times satisfies the classical separation principle of using an inner servo loop.

The resulting performance is illustrated in Figure 4. The attitude response is shown in Figure 4(a) where after the initial detumble period the attitude tracking error decay approaches an exponential behavior as expected from the outer attitude loop control analysis. The rate tracking errors $\delta\boldsymbol{\omega}$ expressed in Eq. (23) as shown in Figure 4(b). For about the first minute the reference angular rate (dashed lines) of the outer loop is requesting about $\omega_{\max} = 1.0$ deg/s for each axes. As the attitude errors are reduced, the requested rates decrease exponentially. As the spacecraft is initially tumbling in approximately the opposite direction of the outer-loop reference rates , the servo loop has to initially aggressively arrest this tumble and then asymptotically track the desired rates. This initial effort is also seen in the saturated reaction wheel motor torques shown in Figure 4(c).

Finally, as an unmodeled body-fixed external torque is included in the simulation, this simulation illustrates that the integral feedback in the rate servo successfully provides robust to such a disturbance and still yields exponential convergence. However, as with any angular momentum based control system compensating for an external torque, the reaction wheel speeds must continue to grow over time as is illustrated in Figure 4(d).

To illustrate the impact of the integral feedback term in the rate servo control, the above simulation is repeated with the integral feedback turned off. The resulting performance is shown in FIgure 5. The rate tracking in Figure 5(b) is no longer asymptotic due to this unmodeled disturance, and the attitude tracking is now only bounded (i.e. Lagrange stable) as illustrated in Figure 5(a).

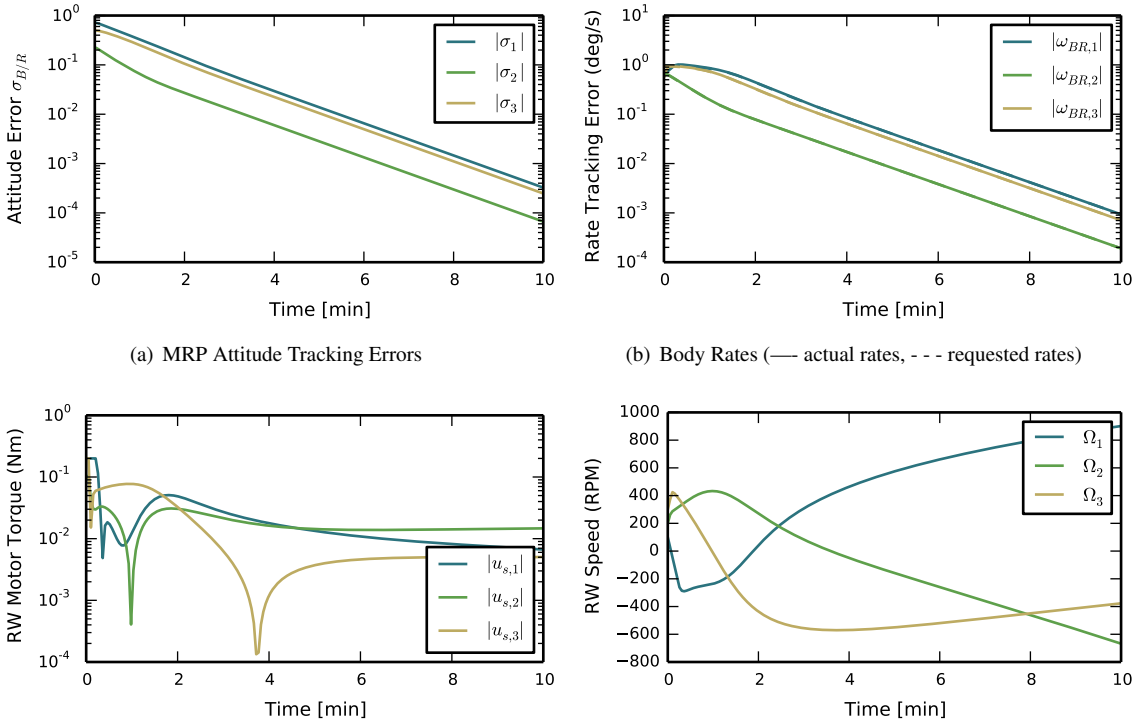

(a) MRP Attitude Tracking Errors

(b) Body Rates (—- actual rates, - - - requested rates)

(c) Reaction Wheel Motor Torques

(d) Reaction Wheel Speeds

Fig. 4: Large Attitude Stabilization using Unknown External Torque.

5.3 Aggressive Outer Loop Gains that Violate the Separation Principle

Next a simulation is run where the outer-loop is set to have a much more aggressive response to attitude tracking errors. This might be required during an orbit trajectory correction control burn sequence where the thruster heading must be maintained within a small margin. The nominal simulation setup in Table 1 is reused here, but K_1 is increased to a value of 2.2. This results in the outer loop having a decay time constant (see Eq. (22)) of 1.2 seconds, smaller then the rate servo control loop time constant of 1.85 seconds (see Eq. (40)).

In this scenario the linearized stability analysis predicts an unstable response if an unmodified control implementation of Eq. (30) is employed. To numerically illustrate this behavior, the simulation is run with the smaller initial state errors $\boldsymbol{\sigma}_{\mathcal{B}/\mathcal{R}}(t_0) = (0.001, 0.002, -0.003)$ and $\boldsymbol{\omega}_{\mathcal{B}/\mathcal{R}} = n\hat{\boldsymbol{\imath}}_h$ are used to study the local small departure stability. As predicted in the analysis, violating the separation principle with this steering and servo control yields a locally unstable response. As the full nonlinear equations are being simulated, the attitudes do not drive towards infinity, but rather are stabilized in a limit cycle through the nonlinear contributions as illustrated in Figures 6(a) and 6(b).

However, if the $\boldsymbol{\omega}'_{\mathcal{B}^*/\mathcal{R}}$ term in Eq. (30) is removed, then the linear stability analysis predicted a locally stable response even with this aggressive outer loop. Figures 6(c) and 6(d) illustrate the resulting converging performance. The requested and actual rates don't converge in this scenario, but this is not expected in this setup. The overall response is locally asymptotically stable, however, as predicted by the linear stability analysis. In essence, by removing the $\boldsymbol{\omega}'_{\mathcal{B}^*/\mathcal{R}}$ term the attitude steering control reverts to a more classical feedback control. While the asymptotic stability is only analytically predicted for small departures, numerical simulations with large departures indicate always resulting in a stable response as well.

6. Conclusions

This paper discusses a two-stage attitude control implementation where an outer guidance loop uses the attitude tracking errors to develop the desire body rates relative to a time varying reference frame, and then an inner servo loop seeks to track these rate commands. This allows for three-dimensional attitude response to be shaped through rate commands similar to how may robotic systems are controlled. The presented Modified Rodrigues Parameter (MRP) and principal rotation parameter based steering laws provide convenient smoothly saturation behaviors for large angular motions resulting in the spacecraft reaching a predictable maximum coast rate to approach

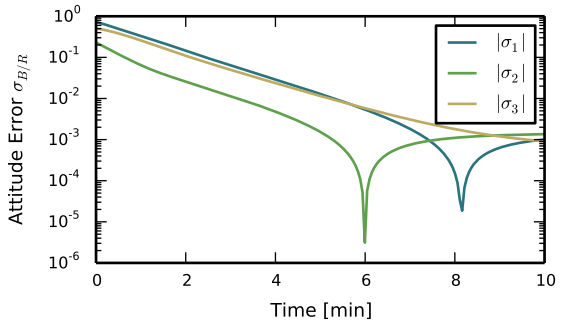

(a) MRP Attitude Tracking Errors

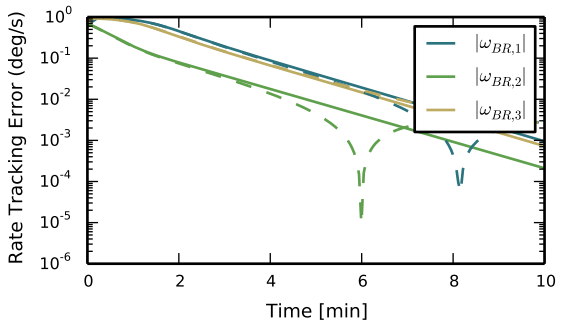

(b) Body Rates (—- actual rates, - - - requested rates

Fig. 5: Large Attitude Stabilization using Unknown External Torque Without Integral Feedback.

a target orientation. This large-scale rotation behavior is then coupled with a tunable linear response behavior for rotations close to the reference frame, resulting in the closed-loop tracking error decaying exponentially. The servo loop musts satisfy the separation principle to provide overall stability. It is implemented to asymptotically track a desired rate command history. Robustness to unmodeled torques is achieved by including an integral rate error measure into the nonlinear rate servo loop. A benefit of this approach is that the shown rate servo can readily be replaced with alternate rate servo solutions. Finally, if the outer loop decay time is more aggressive than the inner loop a simple modification is presented that still leads a stable closed loop response.

REFERENCES

[1] Bong Wie. *Space Vehicle Dynamics and Control*. AIAA Education Series, Reston, VA, 2nd edition, 2008.

[2] Hanspeter Schaub, Maruthi Akella, and John L. Junkins. Adaptive control of nonlinear attitude motions realizing linear closed loop dynamics. *AIAA Journal of Guidance, Control, and Dynamics*, 24(1):95–100, January–February 2001.

[3] Hanspeter Schaub and John L. Junkins. Stereographic orientation parameters for attitude dynamics: A generalization of the rodrigues parameters. *Journal of the Astronautical Sciences*, 44(1):1–19, 1996.

[4] Hyochoong Bang, Min-Jea Tahk, and Hyung-Don Choi. Large angle attitude control of spacecraft with actuator saturation. *Control Engineering Practice*, 11(9):989 – 997, 2003.

[5] Unsik Lee and Mehran Mesbahi. Feedback control for spacecraft reorientation under attitude constraints via convex potentials". *IEEE Transactions on Aerospace and Electronic Systems*, 50(4):2578 – 2592, 2014.

[6] Matthew C. VanDyke and Christopher D. Hall. Decentralized coordinated attitude control of a formation of spacecraft. *AIAA Journal of Guidance, Control, and Dynamics*, 29(5):1101–1109, 2006.

[7] Russell A. Paielli and Ralph E. Bach. Attitude control with realization of linear error dynamics. *AIAA Journal of Guidance, Control, and Dynamics*, 16(1):182–189, Jan.–Feb. 1993.

[8] Hanspeter Schaub and John L. Junkins. *Analytical Mechanics of Space Systems*. AIAA Education Series, Reston, VA, 3rd edition, 2014.

[9] S. R. Marandi and V. J. Modi. A preferred coordinate system and the associated orientation representation in attitude dynamics. *Acta Astronautica*, 15(11):833–843, 1987.

[10] Panagiotis Tsiotras. New control laws for the attitude stabilization of rigid bodies. In *13th IFAC Symposium on Automatic Control in Aerospace*, pages 316–321, Palo Alto, CA, Sept. 12–16 1994.

[11] Yoshihiko Nakamura and Hideo Hanafusa. Inverse kinematic solutions with singularity robustness for robot manipulator control. *Journal of Dynamic Systems, Measurement, and Control*, 108(3):163–171, 1986.

[12] Y. Kanayama, Y. Kimura, F. Miyazaki, and T. Noguchi. A stable tracking control method for an autonomous mobile robot. *Robotics and Automation,*, 1:384–389, May 1990.

[13] Shriram Krishnan and Srinivas R. Vadali. An inverse-free technique for attitude control of spacecraft using cmgs. *Acta Astronautica*, 39(6):431–438, 1997.

[14] Hanspeter Schaub, Srinivas R. Vadali, and John L. Junkins. Feedback control law for variable speed control moment gyroscopes. *Journal of the Astronautical Sciences*, 45(3):307–328, July–Sept. 1998.

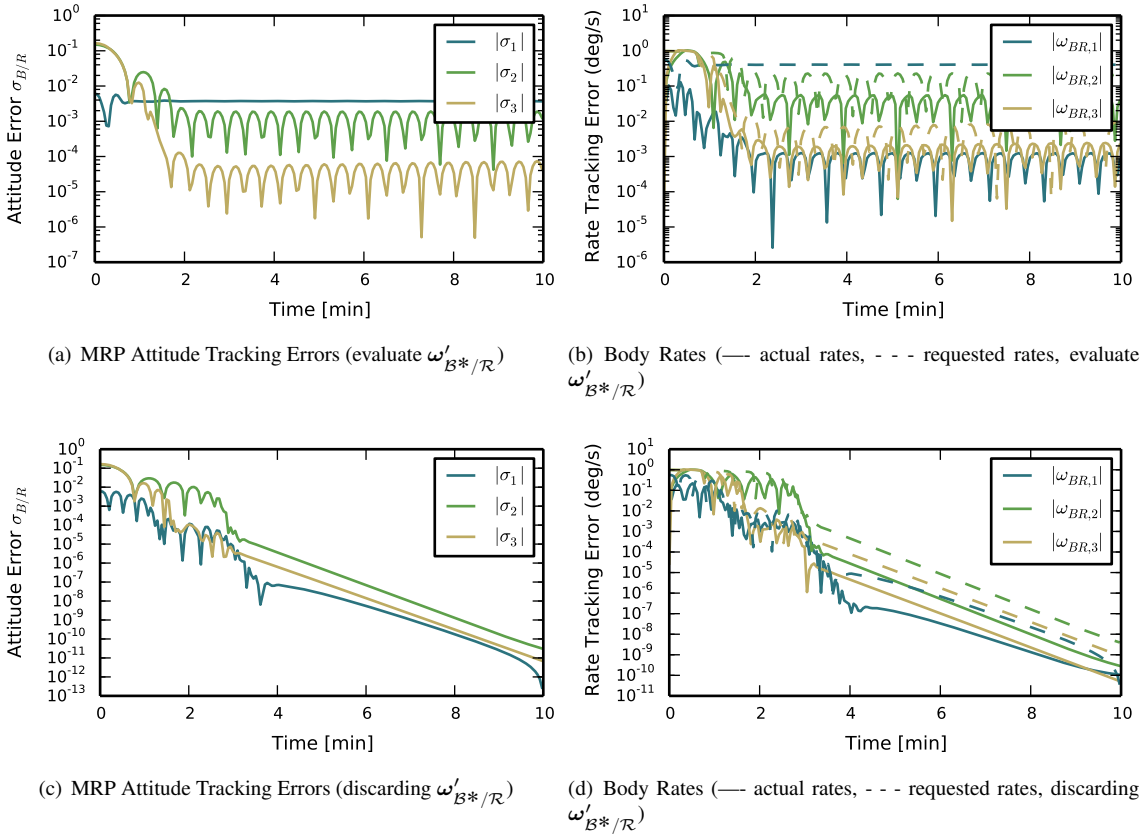

(a) MRP Attitude Tracking Errors (evaluate $\boldsymbol{\omega}'_{\mathcal{B}^*/\mathcal{R}}$)

(b) Body Rates (—- actual rates, - - - requested rates, evaluate $\boldsymbol{\omega}'_{\mathcal{B}^*/\mathcal{R}}$)

(c) MRP Attitude Tracking Errors (discarding $\boldsymbol{\omega}'_{\mathcal{B}^*/\mathcal{R}}$)

(d) Body Rates (—- actual rates, - - - requested rates, discarding $\boldsymbol{\omega}'_{\mathcal{B}^*/\mathcal{R}}$)

Fig. 6: Small Attitude Stabilization Violating the Inner/Outer Loop Separation Principle Using No External Torque.

[15] Kevin A. Ford and Christopher D. Hall. Singular direction avoidance steering for control-moment gyros. *AIAA Journal of Guidance, Control, and Dynamics*, 23(4):648–656, 2000.

[16] Henzeh Leeghim, Hyochoong Bang, and Jong-Oh Park. Singularity avoidance of control moment gyros by one-step ahead singularity index. *Acta Astronautica*, 64(9–10):935–945, May–June 2009.

[17] Bong Wie. Singularity escape/avoidance steering logic for control moment gyro systems. *AIAA Journal of Guidance, Control, and Dynamics*, 28(5):948–956, 2005.

[18] Nazareth S. Bedrossian. *Steering Law Design for Redundant Single Gimbal Control Moment Gyro Systems*. M.S. Thesis, Mechanical Engineering, Massachusetts Institute of Technology, Boston, MA, Aug. 1987.

[19] Hassan K. Khalil. *Nonlinear Systems*. Prentice-Hall, Inc., Upper Saddle River, NJ, 3rd edition, 2002.

[20] Ki-Seok Kim and Youdam Kim. Robust backstepping control for slew maneuver using nonlinear tracking function. *IEEE Transactions on Control Systems Technology*, 11(6):822–829, 2003.

[21] Manuel Diaz-Ramos and Hanspeter Schaub. Kinematic steering law enabling conically constrained spacecraft attitude control. In *AAS Guidance, Navigation and Control Conference*, Breckenridge, CO, Feb. 2–8 2017. Paper AAS 17-024.

[22] Mar Cols Margenet, Hanspeter Schaub, and Scott Piggott. Modular attitude guidance development using the basilisk software framework. In *AIAA/AAS Astrodynamics Specialist Conference*, Long Beach, CA, Sept. 12–15 2016.

[23] John Alcorn, Hanspeter Schaub, Scott Piggott, and Daniel Kubitschek. Simulating attitude actuation options using the basilisk astrodynamics software architecture. In *67th International Astronautical Congress*, Guadalajara, Mexico, Sept. 26–30 2016.